Rhythmic sampling of multiple decision alternatives in the human brain

Marcus Siems[1], Yinan Cao[1], Maryam Tohidi-Moghaddam[1], Tobias H. Donner[1], & Konstantinos Tsetsos[1,2]

[1] Department of Neurophysiology and Pathophysiology, University Medical Center Hamburg-Eppendorf, Hamburg, Germany

[2] School of Psychological Science, University of Bristol, Bristol, United Kingdom

Contact Information

Correspondence: m.siems@uke.de & k.tsetsos@bristol.ac.uk

Highlights

- Humans navigate complex decisions by dynamically shifting their attention to sequentially sample different aspects of the decision problem.
- Using magnetoencephalography (MEG), we tracked the locus and strength of covert attention in humans performing a multialternative choice task.
- The strength of covert attention fluctuated rhythmically at 11 Hz, independent from oculomotor activity.
- At the peak of the 11 Hz attentional oscillation, the previously sampled alternative was resampled, while at the trough of the oscillation, sampling switched to a different alternative

Summary

Humans and other animals navigate real-world decisions by sequentially attending to (*sampling*) subsets of the available information. The neural mechanisms underlying the selective sampling of decision-relevant information remain unknown. Here we used magnetoencephalography (MEG) recordings and neural decoding to track the spontaneous dynamics of the locus and strength of covert attention as human participants performed a three-alternative perceptual choice task. The strength of covert attention fluctuated rhythmically at 11 Hz. At the peak of this oscillation, attention re-focused on the location of the previously sampled alternative, promoting the in-depth evaluation of a single alternative. By contrast, at the trough, attention was oriented to a different alternative, that way facilitating the comparison between alternatives. Further, switching attention to a different alternative intrinsically reset the attentional oscillation. We propose that rhythmic attentional sampling is a universal cognitive mechanism underpinning the flexible information processing necessary for key decision computations.

Introduction

Every day of our lives we make several decisions based on varying amounts of external information. Research in psychology and neuroscience has described the mechanisms underlying simple sensorimotor decisions, where the amount of decision-relevant information typically falls within the processing capacity of the cognitive system[1-3]. However, the computational and neural mechanisms of more complex decisions (e.g. real-life decisions involving multiple attributes and alternatives) remain largely unknown[4]. This is because – unlike in simple sensorimotor decision tasks where incoming sensory information can seamlessly flow to downstream computations – in more complex decisions, the brain may not be able to parse and process all decision-relevant information in parallel. Thus, subsets of the available information may need to be sampled serially as the decision unfolds. For instance, when choosing between different apartments, one might examine one of the available alternatives on a single relevant aspect (such as price, size, distance to city center, etc.) at each moment in time, later shifting focus to a different attribute or alternative[5-8].

Information sampling via attentional mechanisms may thus be a key aspect of complex, naturalistic decision-making, dynamically shaping the input that feeds into the underlying computation[9-11]. Then, the ability to track the spontaneous and internal dynamics of information sampling during decision formation is critical for identifying the input to the decision computation. However, current neurophysiological approaches to decision-making have ignored these internal sampling dynamics, which results in underdetermined mechanistic inferences about decision computations. Here, we harnessed the high temporal and spatial resolution of MEG recordings to continuously track the locus and strength of covert spatial attention during multialternative decisions.

Our approach showed that during the strength of covert attention decision formation oscillates at 11 Hz. Refocusing attention to the previously sampled alternative occurs at the peak of this oscillation while switching to a different alternative occurs at

the trough and resets the ongoing oscillation. Thus, the conflict between gathering additional information about an alternative and exploring other alternatives is temporally resolved through rhythmic sampling[12-18]. We propose that rhythmic attentional sampling is a universal mechanism that supports the flexible information processing needed to perform cognitive tasks with increased processing demands.

Results

We recorded non-invasive MEG from a total of 20 participants (9 female, age_{mean} = 28.05 years ± age_{STD} 4.6 years). The participants performed two interleaved tasks: A three-alternative perceptual choice task at threshold discriminability (main task) and a flicker-detection task (sensory localizer; see Methods). Our experimental protocol for the main task followed a three-alternative forced choice design with a fixed response window (Figure 1A). A trial started with a central fixation, followed by three static Gabor-patches of different contrast levels appeared at 2.2 degree eccentricity. To control for bottom-up sensory capture of attention induced by the presentation of the stimulus, we employed two framing conditions that were randomly assigned on each trial. In particular, in different framing conditions, participants were instructed to either choose the Gabor-patch with the highest or the lowest contrast, with the framing instruction being revealed one second after the stimulus onset. Because the framing manipulation decoupled the low-level features (i.e., contrast) from the task-relevance of the choice alternatives, the task can probe goal-directed (top-down) attention independent from bottom-up sensory cortical responses. Participants performed the task with around 77% accuracy ($range_{min,max}$ = [66%, 86%]; Figure 1B) and there was no accuracy difference between the two task framings ($|t_{19}| = 1.679$; $p > 0.11$).

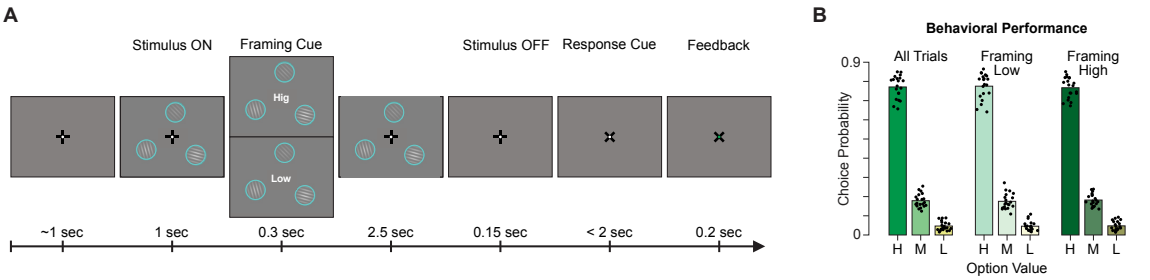

Figure 1. Experimental task & behavioral performance

(A) Trial structure of the three-alternative decision-making task with variable task framing. Stimulus size, contrast and eccentricity are indicative and have been changed for visualization purposes. Participants were asked to select the stimulus that had the highest (framing high: 'Hig') or the lowest (framing low: 'Low') contrast. **(B)** Choice probability across the three alternatives (H, M, L indicates high, medium, low decision value) for all trials and within each framing condition. The dots indicate individual participant's choice probability.

Tracking the locus and strength of covert attention using MEG

We developed an approach to continuously track the locus and strength of covert attention during protracted decision processing. Specifically, we used the sensory localizer trials to train an inverted encoding model[19] on the angular positions of the stimuli. This enabled us to estimate the spatial focus of attention during the decision-making task (Figure 2A and S1). We followed the assumption that the neural representation, i.e. decodability, will be stronger for attended and weaker for unattended targets[20-22]. Inverting the model yielded a time-resolved estimate of the response to each of the three angular positions during the decision-making task (Figure 2B). From the estimated responses we reconstructed spatial attention as the vector sum of the three channel responses (left, top, right). We focused on the resulting vector (referred to as 'Attentional Vector' in the following) to precisely track attentional fluctuations in the brain (Figure 2B). The vector length corresponded to the *strength* of attention and the angular similarity to the three stimulus positions corresponded to the *locus* of attention. We further tracked the eye-gaze position to ensure central fixation and disentangle covert attention allocation from eye-movements.

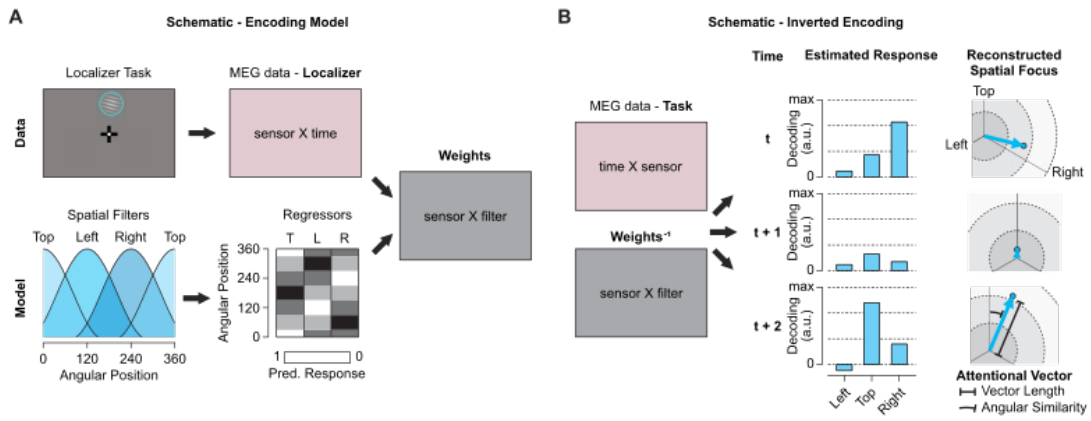

Figure 2. Reconstructing the locus and strength of spatial attention with inverted encoding models
(A) Training the encoding model. The encoding model consists of a set of linear spatial filters defining the response given a certain stimulus. It comprises each information channels tuning curve, which when discretized at presentation angles forms the Design Matrix. In combination with MEG data from the sensory localizer (see Methods) the weighting of the information channels within each MEG sensor can be estimated by solving the general linear model (GLM). **(B)** Inverting the weights to estimate the channel responses during the decision-making task. We multiplied the inverted weighting matrix with the MEG data to estimate the response of the information channels at each time point. From the estimated responses we reconstructed the focus of spatial attention as the vector sum of the three spatial channel responses (left, top, right). The resulting Attentional Vector featured first, the length corresponding to the overall amount of attention and second, the angular similarity to the three stimulus targets.

Attention strength oscillates at 11 Hz

Building on recent work on the neurophysiological basis of attention in simple perceptual tasks[23], we hypothesized that attention strength (i.e., vector length) would vary throughout the course of the trial as a result of the distinct processing demands in the sensory- and decision-phases of the task. In a first step we thus quantified the trial-averaged distribution of the vector length (Figure 3A). After the stimulus onset, attention strength steeply ramps up and, relative to the framing cue onset, displays three peaks at around -0.8 s (close to stimulus onset), 0.2 s (early in the decision phase) and between 0.7-1.2 s (late in the decision phase). For external validation of this metric we compared the distribution of attention strength to the distribution of the pupil diameter, a peripheral measure of task engagement[49,50]. Evoked pupil responses resembled the trial-averaged

attentional vector dynamics, albeit with more sluggish dynamics (Figure 3B; $r_{pupil,veclen}$ = 0.54; p = 0.007).

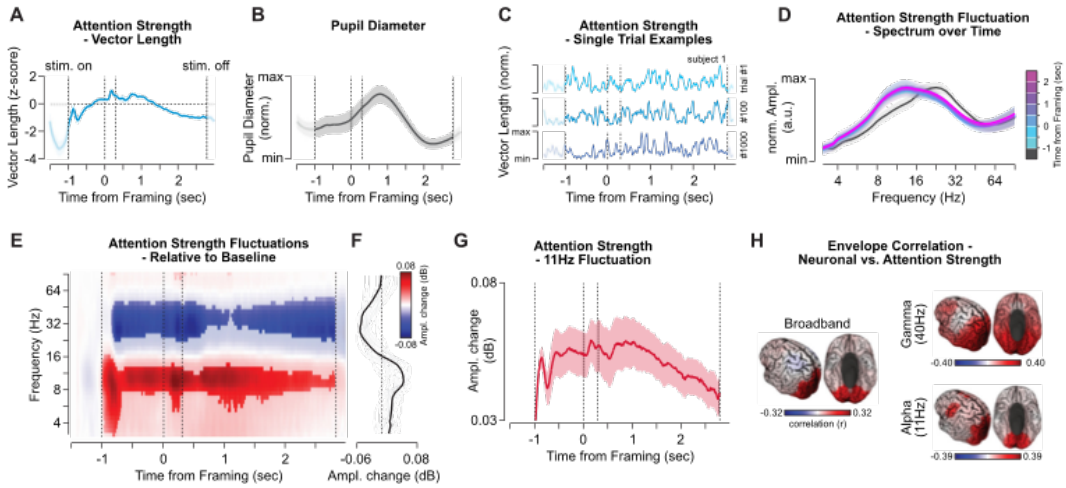

Figure 3. Attention strength fluctuates at around 11 Hz.

(A) The distribution of the z-scored overall attention strength, i.e. vector length. The blue line indicates the average over trials and participants. The shaded area indicates the standard error of the mean (SEM). Vertical dashed lines indicate the stimulus onset, framing cue onset and offset as well as the stimulus offset (from left to right). **(B)** The average normalized pupil diameter during task execution. The thick line and shaded area indicate the average and the SEM over participants. **(C)** Single trial example traces of the normalized attention strength. The depicted trials are from participant 1, session 1. **(D)** Windowed normalized amplitude spectra of attention strength fluctuations over the trial. Lines indicate the participant average, shaded areas display the SEM. The lines are color-coded according to the window onset (0.5 sec. window length) with regard to the framing cue. **(E-G)** Frequency-specific change of attention strength amplitude relative to baseline. The frequency-wise amplitude strength values were normalized by dividing the average amplitude during the 0.5 seconds prior to stimulus onset and displayed in dB. **(E)** Time-frequency resolved (TFR) distribution of the amplitude of attention strength fluctuations. Red and blue colors indicate an increase or decrease relative to baseline, respectively. The values were statistically masked at p_{FDR}< 0.01 within each frequency. Vertical dashed lines were defined as in **(A)**. **(F)** Average frequency-wise amplitude change, as in **(E)**, throughout the stimulus ON period. Thick and thin lines display the average and single participant amplitude changes, respectively. **(G)** Attention strength fluctuation amplitude at 11 Hz, relative to baseline in dB. Same data as in **(C)**. Shaded area indicates the SEM. **(H)** Correlation of the trial averaged amplitude envelopes between the neuronal signal (compare Figure S2) and the attention strength fluctuation. The correlation was computed for the broadband as well as frequency resolved signals. The values were statistically masked at p_{FDR}< 0.05 within each panel.

Importantly, there were substantial fluctuations of attention strength within each trial (Figure 3C), which we quantified using spectral analyses (Figure 3D-G). Attention

strength fluctuated most strongly in the frequency range between 8 - 22 Hz (Figure 3D), with a clear increase from the pre-trial baseline (-1.5 to -1 seconds prior to framing) at 11 Hz, and a decrease between 25 - 45 Hz (Figure 3E and 3F). The increase of the 11 Hz fluctuations was most pronounced between 0.5 seconds prior, up until 1.5 seconds after the framing cue (Figure 3G).

To examine the link between attentional and neural dynamics, we next correlated the time-frequency resolved time courses of the attention strength oscillations (compare Figure 3E) with the trial-averaged neuronal signal amplitude envelope (compare Figure S2) in the respective frequency ranges. Following the spectral properties of attention strength (Figure, 3G) we focused our analysis on the alpha (11 Hz) and gamma (40 Hz) frequencies as well as on the broadband activity. We found strong positive correlations of attention strength with visual cortex activity in alpha, gamma, and broadband activity ($r > 0.25$; $p_{FDR} < 0.05$; Figure 3H). Attention-neuronal correlations in the alpha- and gamma-band further highlighted an extended network of early and ventral stream visual and lateral prefrontal cortical areas (11 Hz and 40 Hz; $p_{FDR} < 0.05$; Figure 3H, right).

The observed attentional fluctuations could be a consequence of stimulus-evoked cortical (and in particular visual) activity[24]. However, conversely to the 11 Hz increase in attention strength, we observed stimulus-evoked suppression of cortical activity in the alpha and neighboring frequency ranges throughout the entire trial duration (Figure S2). Similarly, the raw decoding of the three alternatives (see Figure 2B middle column) displayed a broadband decrease between 8 – 45 Hz (Figure S3). Thus, the increased attentional fluctuation at 11 Hz during the trial was distinct from stimulus induced cortical activity responses.

Attention strength fluctuations correlate with behavioral performance

Attention strength varies throughout the trial and displays prominent band-limited fluctuations but it remains to be shown whether these attention dynamics are relevant for

decision-making performance. To evaluate the behavioral relevance of these dynamics we compared attentional fluctuations between correct and error trials. In the first analysis we found that in correct choices, attention strength (compare Figure 3A) was increased during the late decision phase of the trial (Figure 4A). However, this was a non-significant trend.

In a second analysis we repeated the comparison between correct and error trials by focusing on the frequency resolved attention strength fluctuations (compare Figure 3E). We identified significantly increased attention strength fluctuations related to choosing correctly from 1.5 seconds post framing until the end of the trial, peaking in a frequency range from 8 – 16 Hz ($p_{FDR} < 0.05$). Thus, attention strength fluctuations particularly around 11 Hz might be predictive of choosing the best alternative. Importantly, we matched correct and error trials in nominal difficulty and framing conditions (see Methods).

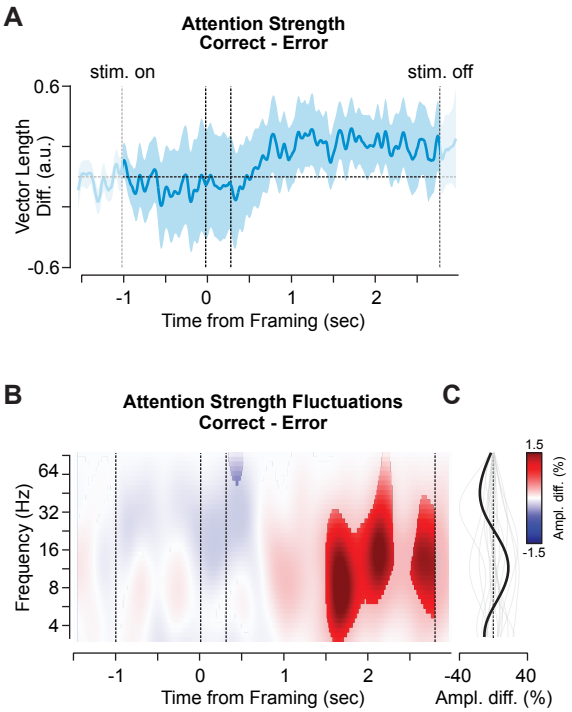

Figure 4. Attention strength fluctuations correlate with performance.

(A) The distribution of the overall attention strength difference, i.e. vector length, between correct and error trials (condition matched, see Methods). The blue line and shaded area indicate the average over participants and the standard error of the mean (SEM). Vertical dashed lines denote the stimulus onset, framing cue onset and offset as well as the stimulus offset (from left to right). **(B-C)** Time-frequency resolved (TFR) attention strength fluctuation differences between correct and error trials as percent change to correct. **(B)** The distribution of TFR amplitude differences (correct-error) over the full spectrum and trial duration. The values were statistically masked at pFDR< 0.05 over the spectrum. **(C)** Frequency-wise amplitude change, as in **(B)**, averaged over the stimulus ON period. Thick and thin lines display the average and single participant amplitude changes, respectively.

Focusing and switching attention nested within an 11 Hz rhythm

The above analyses highlight task-relevant modulations of attention strength at around 11 Hz. However, these findings are unrelated to the locus of attention. Is there a relationship between attention strength and where attention is directed at (attention locus)? Recent theories suggest that when attention is at an oscillatory peak, processing of a selected stimulus is enhanced[14,15,25-27]. By contrast, when at an oscillatory trough,

attention is relatively disengaged and can be shifted from one stimulus to another. Thus, according to this “rhythmic sampling” framework, attention strength is expected to index the stability of the attention locus. In particular, it is expected that when attention is stronger, the tendency to maintain attention on one alternative is also strong (locus stability). When attention is weaker, the tendency to switch to a different alternative increases (locus instability)[17,28,29], with attentional switches occurring swiftly analogously to covert ‘attentional saccades’[16,30,31].

To test this hypothesis directly, we extracted brief events of maximal engagement with one decision alternative and assessed their temporal dynamics. This approach allows us to quantify several aspects of information sampling, such as identifying periods when participants are engaged with a given alternative, or quantifying how long it takes to switch attention between alternatives. Crucially, we can ask if these temporal regularities occur within the 11 Hz attention strength oscillation.

Quantitatively, attentional events are defined as points in time when the Attentional Vector aligns with one of the three decision alternatives (top, left, right). Thus, we focused on the maximum angular similarity (MAS) between the Attentional Vector and the directions of the alternatives (Figure 5A). Hereby, the average attentional locus displays no systematic variations over the course of a trial. Next, we binarized MAS by applying a threshold (MAS at its 90% percentile, see Methods) to define brief events associated with selective attention to a single alternative (akin to an ‘attentional saccade’). It is worth noting that the MAS metric is defined in a circular space and thus under completely random conditions (periods without visual stimulation) or when decodability of the alternatives is weak (complete inattentiveness) MAS will still exceed the angular threshold at random times. In these cases, we would falsely infer that attention is allocated to one of the three alternatives. To avoid this, we thus included a second threshold on the vector length, enabling us to exclude purely noise-driven events as much as possible (Figure 5B and S4). An attentional event is thus only recorded

when both the attention locus is selective at one decision alternative and the attention strength is sufficiently high.

Next, we characterized the dynamics of attentional events in a data-driven fashion. To assess their temporal structure we timed the interval in-between successive attentional events (inter-event-intervals, IEI; Figure 5C). Assuming that attentional allocation is governed by a random Poisson process (i.e., no temporal structure), the IEI histogram would display an exponential decay of probability with interval duration (Figure 5C,D, dashed lines; see Methods). However, we identified clear deviations from this prediction, as the IEI histogram peaked at 0.13 seconds and at around 0.18 seconds ($p_{FDR} < 0.05$; Figure 5C). These short peak latencies indicate that events tend to cluster together in a burst-like pattern over the course of the trial. These results confirm that the temporal structure of attention allocation is not random.

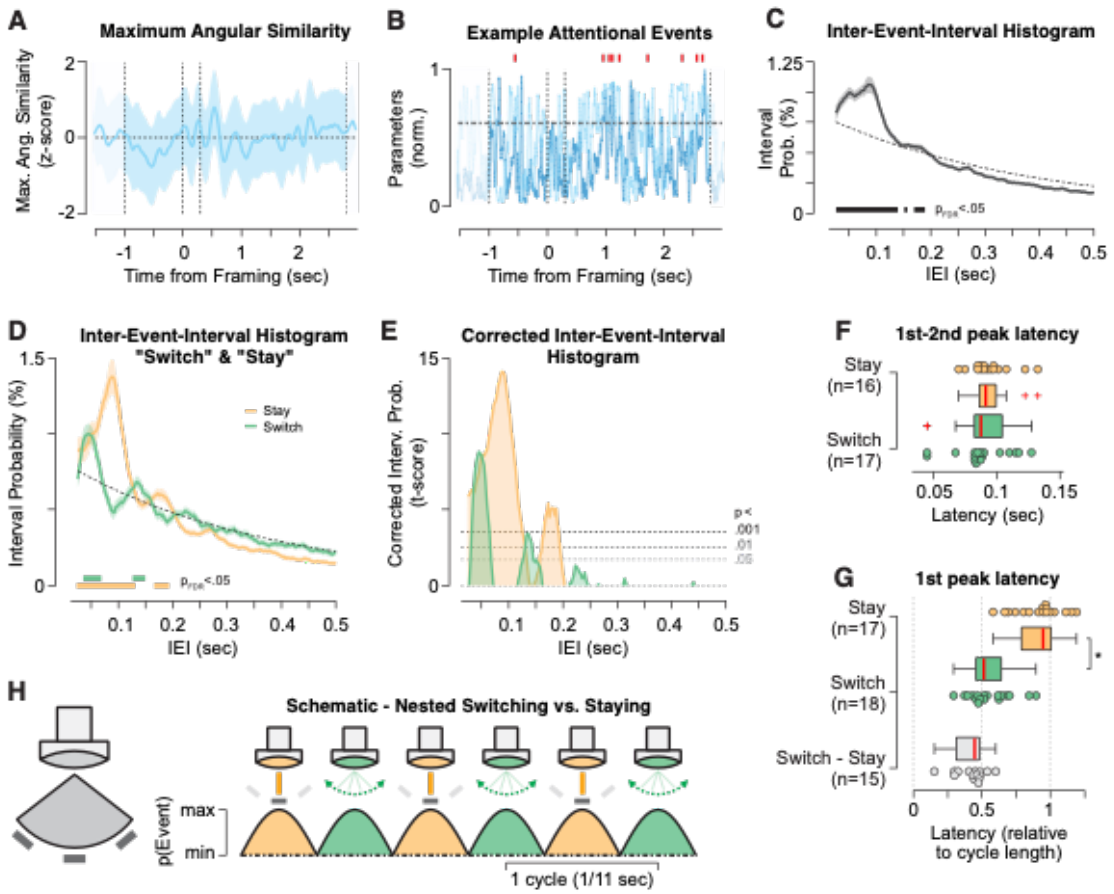

Figure 5. Attention allocation to distinct stimuli is nested within an 11 Hz rhythm.

(A) Maximum angular similarity averaged over trials. The blue line indicates the z-scored average over participants. The shaded area displays the SEM. Vertical dashed lines indicate the stimulus onset, framing cue onset and offset as well as the stimulus offset (from left to right). **(B)** Schematic definition of attentional saccades in an example trial. An attentional saccade (red mark) is recorded when vector orientation (90% MAS percentile) and attention strength are sufficiently high (90% vector length percentile). **(C)** Inter-event-interval (IEI) probability histograms over all trials and attentional events. The black line indicates the average over participants, the shaded area the SEM. The black bars denote significant ($p_{FDR} < 0.05$) interval probabilities exceeding random conditions (dashed line). **(D)** Inter-event-interval histograms separately for stay (orange line, ± SEM) and switch (green line, ± SEM) attentional events. The bars denote significant ($p_{FDR} < 0.05$) interval probabilities exceeding random conditions. **(E)** Same data as in **(D)** plotted as t-score against random. Dashed lines indicate the uncorrected significance-levels and zero. **(F)** Box-plots of first-to-second peak latencies. Colored dots display single participants, color-coded as above. **(G)** First peak latency relative to the cycle length (see **(F)**). Asterisk denotes a significant difference between event types ($p_{FDR} < 10^{-4}$). N denotes the number of participants with significant peaks within the IEI histogram. **(H)** Schematic - Covert attention "spotlight" allocations, i.e. attentional saccades, nested within the underlying 11 Hz rhythm with two sets of attentional events offset by half a cycle: “staying” on the same stimulus and “switching” the focus of attention.

We next examined whether the dynamics of attentional allocation change as a function of the identity of the previously attended alternative. Attention can either re-focus on the previously attended alternative (staying) or shift to a different alternative (switching). As evident in the corresponding IEI histograms, staying and switching events exhibited distinct temporal profiles: staying predominantly occurred after 0.1 s and 0.18 s from the preceding event; and switching mostly after 0.05 s and 0.15 s (Figure 5D and 5E). Generally, we observed more stay than switch events (mean p_{Stay} = 0.63, $p_{Stay,25\%-75\%}$ = 0.60 – 0.64) and that switching was relatively increased right after stimulus onset and later in the decision phase (Figure S5). We postulate that the increased "switch rate" later in the decision suggests that more comparative processing takes place closer to the response. Similarly, the stronger and more sustained "stay rate" early-on in the decision can be mapped to the independent evaluation of the different alternatives[32]. This pattern is consistent with the standard multistage neuroeconomic framework, according to which valuation precedes comparative computations.

The IEI histograms associated with stay and switch events can help assess the (potential) rhythmicity of these events: Assuming that events likely occur at distinct phases of an underlying rhythm, we can expect phase-specific peaks of IEI probability reappearing in the first, second, third, etc. cycle of a putative oscillation. Thus, the latency between reappearing peaks in the IEI histogram (effectively the cycle length) would enable us to quantify rhythmicity. Both staying and switching events displayed approximately 0.09 s first-to-second peak latencies ($median_{stay}$ = 0.09 s, $range_{stay,25\%-75\%}$ = 0.088 s – 0.098 s; $median_{switch}$ = 0.088 s, $range_{switch,25\%-75\%}$ = 0.08 s – 0.095 s) – corresponding to rhythmicity at 11 Hz (Figure 5F). This is the same frequency we identified as the dominant attention strength fluctuation (Figure 3), which indicates that both event types might be nested within this oscillation (Figure 5H).

We further observed a prominent offset between switch and stay peak probabilities (Figure 5D and 5E). While stay events displayed the first peak at around

0.85 s (median = 0.85 s, $range_{25\%-75\%}$ = 0.76 s – 0.94 s), switch events peaked earlier at around 0.45 s (median = 0.46 s, $range_{25\%-75\%}$ = 0.41 s – 0.54 s). With respect to each participant's putative oscillation frequency (Figure 5F) we identified the first 'switching' peak at around 0.5 (median = 0.51 cycle length, $range_{25\%-75\%}$ = 0.46 - 0.64) and the first 'staying' peak at a full cycle length (median = 0.95 cycle length, $range_{25\%-75\%}$ = 0.79 - 1.01) relative to the previous event (Figure 5G), with a consistent switch-to-stay phase-shift slightly below half a cycle (median difference = 0.45 cycle length, $range_{25\%-75\%}$ = 0.31 - 0.48; Figure 5G, grey box).

In sum, the temporal regularities characterizing attentional events provided a deep window into the dynamics of covert attentional sampling during decision formation. These results show that both event types can occur probabilistically at distinct phases of the ongoing attention oscillation, half a cycle apart (Figure 5G and 5H).

Brief attentional saccades impact the ongoing attention strength fluctuation

The offset between switch and stay events introduces an insightful caveat. We would expect that events, irrespective of their history, are falling out from the ongoing 11 Hz oscillation. This naïve model leads to a specific prediction when taking longer sequences of events into account: We would expect switching to cluster around half a cycle after a previous stay event or a full cycle after a switch event (Figure 6A). Thus, we would expect IEI peaks at double the oscillation frequency and no offset between switch- and stay events (Figure 6A, lower panel). In principle, our diverging findings (Figure 5G) could be still consistent with the naïve model if stay events occur more often.

However, the naïve model does not hold when we directly assess longer event sequences. We defined IEI histograms for four sequence types: Switch after stay, switch after switch, stay after stay, stay after switch. We found that the IEI probabilities within each event type were invariant to the preceding event type (Figure 6B and 6C). In other words, the higher likelihood of stay events cannot explain away the first peak offset

between stay and switch events (Figure 5G). Instead, the oscillation cycle appears to start anew no matter which event occurred last.

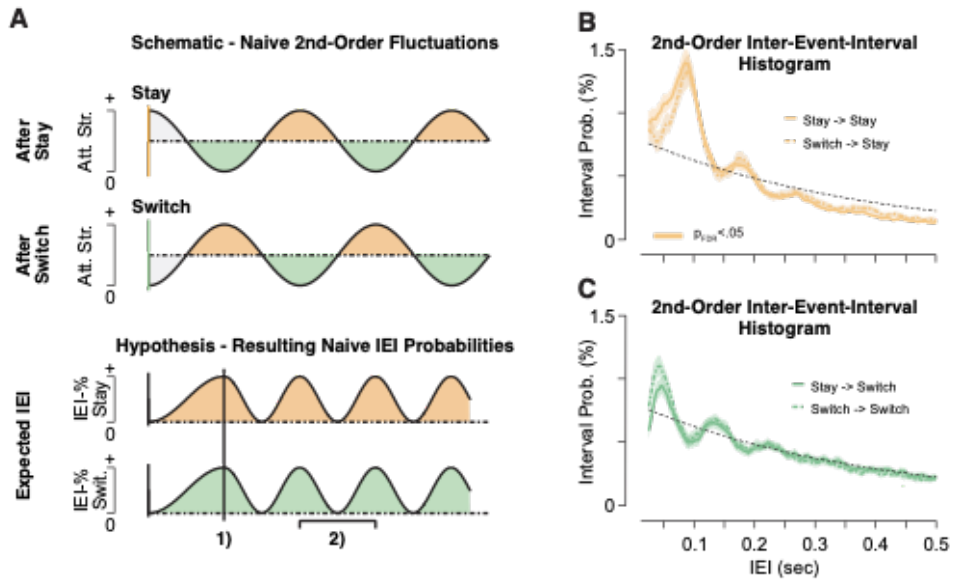

Figure 6. Schematic and empirical second-order sequence inter-event-interval probabilities.
(A) Schematic of IEI probability depending on previous event identity. If the attention oscillation persists irrespective of events (naive model), we would expect **1)** no offset between stay and switch peaks and ***2)*** peak event probabilities to fluctuate at double the attention modulation frequency (Figure 3E vs. Figure 5F). **(B-C)** Second-order sequence effects on inter-event-interval probabilities separately for **(B)** stay (orange line, ± SEM) and **(C)** switch (green line, ± SEM) attentional events. Solid and dashed colored lines indicate the mean interval probability following a stay or a switching event, respectively. The bars denote significant ($p_{FDR} < 0.05$) interval probabilities differences between respective 2nd-order sequence types, color-coded as above. The empirical data is not in line with the naive model **(A)**.

Taken together, this finding challenges the concept that the attentional oscillation is unaltered in amplitude and frequency over time (Figure 5H). Attentional events do not merely fall out from but interact with the attentional strength oscillation in a way that we illuminate further in the below.

Attentional switching resets rhythmic attention strength fluctuations

To better understand how attentional events might be affecting the attentional oscillation we focused on attention strength around the onset of these events. We averaged

attention strength in a time-window from -0.2 s prior to 0.2 s after each event (Figure 7A and 7B; and Figure S7 for maximum angular similarity). Prior to an event, the traces of attention strength were relatively consistent over participants but largely unaligned between switch and stay (mean r_{pre} = 0.13, $r_{pre,25\%-75\%}$ = -0.05 - 0.34; t_{19} = 0.49, p = 0.31; correlations on detrended signals, compare Figure 7B). By contrast, right after the event, the attention strength traces indicated synchronization around event onset (mean r_{post} = 0.60, $r_{post,25\%-75\%}$ = 0.54 – 0.76; t_{19} = 2.59, p = 0.009; correlations on detrended signals). Moreover, attention strength was generally weaker around switching- compared to stay events both pre- (mean $ratio_{Switch/Stay}$ = 0.90, $range_{25\%-75\%}$ = 0.85 – 0.94; t_{19} = -8.09, $p < 10^{-6}$; Figure 7C) and post-event (mean $ratio_{Switch/Stay}$ = 0.92, $range_{25\%-75\%}$ = 0.88 – 0.95; t_{19} = -7.40, $p < 10^{-6}$) but increased post-event by almost 2% (mean $\Delta ratio_{Switch/Stay}$ = 0.019, $range_{25\%-75\%}$ = 0.011 – 0.029; t_{19} = 7.21, $p < 10^{-6}$).

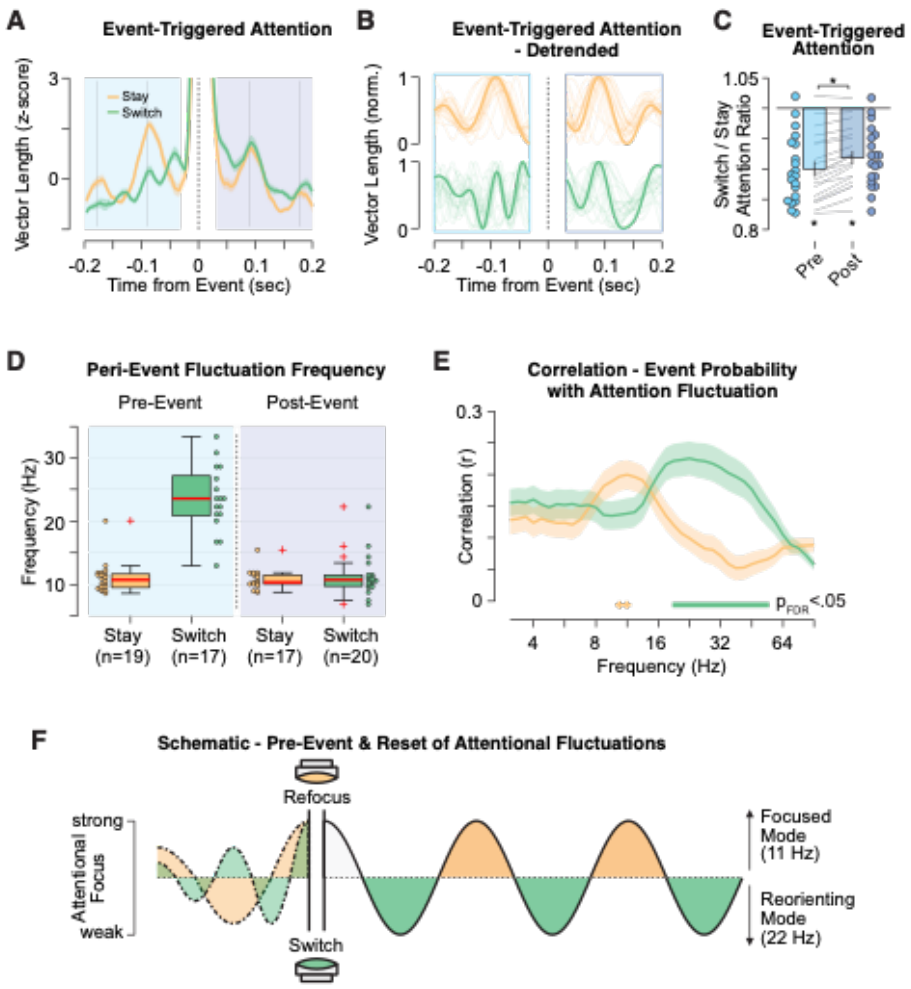

Figure 7. Peri-event fluctuations of attention strength.

(A) Attentional event-triggered average of the z-scored attention strength, i.e. vector length. The colored lines and shaded area indicate the average and SEM over events and participants separately for stay (orange) and switch events (green). Pre- and post-event epochs are highlighted in blue and purple. Gray lines display full 11 Hz cycles from the event. **(B)** The same data as in **(A)** detrended individually pre- (-0.2 s to -0.05 s) and post-event (0.05 s to 0.2 s). **(C)** Peri-event attention strength difference between switch and stay, displayed as the ratio of average activity over a time-window from -0.15 to -0.05 (Pre, blue) and 0.05 to 0.15 (Post, purple). Colored dots and gray lines indicate the single-participant ratio and the difference from pre- to post-event, respectively. Asterisks indicate significant differences ($p < 10^{-6}$). **(D)** Dominant peri-event fluctuation frequencies based on **(B)**. *N* denotes the number of participants for which a sine-fit was possible. **(E)** Correlation between the attentional event probability (Figure S5) and the amplitude of the attentional fluctuations (Figure 3E) over the stimulus ON period. Lines depict the average, shaded areas the SEM over participants. Thick lines indicate significant differences ($p_{FDR} < 0.05$) and crosses a statistical trend for significance ($p_{FDR} < 0.1$). **(F)** Schematic - pre-event activity dissociation and the reset of attentional fluctuations at each event.

Focusing on pre-event attention strength, we observed a faster fluctuation for switch events (Figure 7A and 7B). We thus quantified the dominant fluctuation frequencies pre- and post-event, and for both event types. Attention strength fluctuated at around 11 Hz before and after staying events, as well as after switching events (Figure 7D). However, prior to switching, there was a prominent increase ($p < 10^{-6}$) of the fluctuation frequency to around 22 Hz, dissociating switch and stay events. Correlations between event distributions over the trial and band-limited neuronal activity further underline this qualitative dissociation between switch and stay events in an extended visual and lateral prefrontal cortical network (Figure S8). Overall, our findings suggest that in particular switching events 'reset' the ongoing attention oscillation to the attentional up-state (the focused mode): post-event activity is synced between event types restarting the dominant 11 Hz (Figure 7A and 7B) and attention strength peaks at around 0.09 s and 0.18 s post-event, i.e. approximately after one and two full cycles. On the other hand, the evident desynchronization between pre-switch and pre-stay attention strength can be largely explained by a higher frequency profile preceding switches (Figure 7D).

Given the presence of a higher frequency attentional oscillation prior to switching, we next asked whether faster or slower attention strength fluctuations predict the occurrence of switch or stay events. We thus correlated the attention strength fluctuation amplitude in each frequency range (compare with Figure 3E) with the event probability over the course of the trial (Figure S5). A stronger 11 Hz attention modulation predicted more stay events (Figure 7E, orange line, $p_{FDR} < 0.08$) and a stronger modulation between 19 - 40 Hz more switch events (Figure 7E, green line, $p_{FDR} < 0.05$). Hence, faster attention strength dynamics prior to switching the locus of attention generally corresponded to the appearance of high-frequency modulations of attention strength throughout the trial.

Taken together, our results suggest that switching the attention focus exhibited a unique relation to the attention strength fluctuation (Figure 7F), reciprocally interacting with the fluctuation itself (reset), as well as distinct spectral fingerprints particularly highlighting higher frequencies (> 11 Hz). Attentional switches, embedded in down-phases of attention oscillating at 11 Hz, thus display a distinct neurophysiological mechanism able to resolve the conflict between prolonged focusing on one decision alternative and the need to shift attention between alternatives to compare them.

Dynamics of covert attention can be dissociated from (micro)saccadic eye movements

Previous research has shown that overt, i.e. eye-movements, and covert attention are linked[33-38]. Particularly, it has been proposed that (micro)saccades are overt manifestations of covert attentional processing[33-35]. Similarly, the recent literature on the interplay between attention and decision-making has predominantly focused on overt attention via saccadic eye movements[9-11,39-41]. However, new findings indicate that overt and covert attention allocations can dissociate and might thus be distinct windows onto information sampling and intrinsic processing[31,38]. We thus ask if and how the rhythmic fluctuations of covert attention might relate to the dynamics of the oculomotor system and whether (micro)saccadic eye-movements show compatible dynamics as covert shifts of attention?

We applied eye-tracking and extracted oculomotor events[38], i.e. (micro)saccadic eye-movements (MS), to evaluate the contributions of overt gaze to our measures of covert attention. The trial-averaged MS rate displayed pronounced variation with the trial structure (Figure 8A) increasing after stimulus- and framing cue onset each following a 0.2 s suppression period. To characterize the temporal structure of (micro)saccades, we computed the inter-saccade-intervals (ISI) over the stimulus period. ISI histograms displayed a single peak at around 0.25 s (Figure 8B) and thus considerably longer first-

peak latencies as covert attention events (compare Figure 5D-G; $p < 10^{-10}$). Moreover, due to the lack of additional local maxima, there is no evidence of rhythmicity in the (micro)saccade distribution (i.e. absence of first-to-second peak latencies).

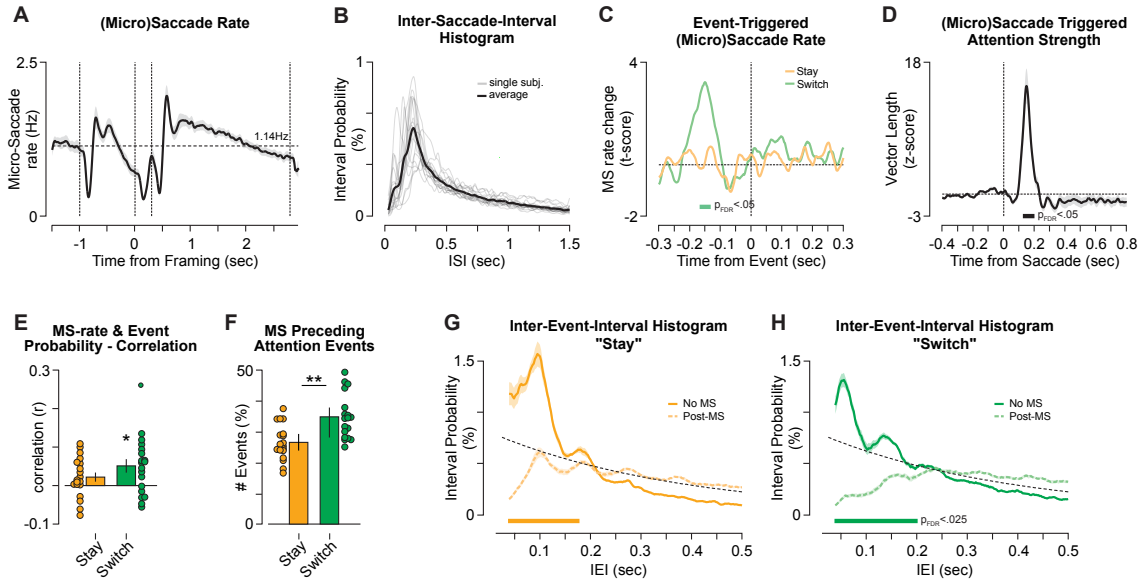

Figure 8. Relationship between covert attentional fluctuations and oculomotor activity.
(A) Average (micro)saccade (MS) rate during task execution. The thick line indicates the average over participants and the shaded area the SEM. Vertical dashed lines indicate the stimulus onset, framing cue onset and offset as well as the stimulus offset. The horizontal line indicates the average MS rate over the stimulus on period (1.14 Hz). **(B)** Inter-saccade-interval histograms for micro(saccades). Thick and thin lines display the group-average and single-participant ISI histograms, respectively. **(C)** Oculomotor event , i.e. (micro)saccade, rates pre- and post-attentional saccades (switch in green, stay orange) tested against shuffled events (t-test). The thick colored bar denotes statistical significance ($p_{FDR} < 0.05$). **(D)** Attention strength around (micro)saccade onset. The data is z-scored based on the 0.4 seconds prior to MS. The black line indicates the average over participants and the shaded area the SEM. The thick bar denotes statistical significance from zero ($p_{FDR} < 0.05$). **(E)** The correlation of the attentional event probability (Figure S5) with the trial-averaged (micro)saccade rate (A) for each participant. The bars and vertical lines display the average and SEM over participants, respectively. The colored dots represent the single participant Pearson correlation coefficients. The dots and bars are color-coded as in (C). Asterisk denotes significant correlations ($|r| > 0$, $p = 0.02$). **(F)** Proportion of attentional events preceded by (micro)saccades. Color-coded as above. Bars and vertical black lines display the mean and 25%-75% range. Asterisk denotes significant difference between switch and stay ($p < 0.001$). **(G-H)** Inter-event-interval histograms for stay **(F)** and switch **(H)** attentional events split into events with (dashed) and without a (micro)saccade (solid line) between successive events. Color-coded as above. The thick colored bar denotes statistical significance (No MS > post-MS; $p_{FDR} < 0.025$).

To directly assess the relationship between oculomotor activity and covert attentional events, we computed the (attentional) event-triggered MS rate. We identified a prominent increase around 0.15 s, exclusively before switching events (Figure, 8C; $p_{FDR} < 0.05$). Conversely, attention strength was strongly increased following a (micro)saccade at around 0.17 s post-saccade (Figure 8D). Correlating the average MS rate over the trial with the corresponding attentional event probabilities within each participant (Figure 8E), we found that attention switches are positively correlated with the MS rate ($r = 0.06$; $p = 0.02$). Further, we found that (micro)saccades preceded switching events (mean = 35%, range = 25 – 50%) more often than staying events (mean = 26%, range = 17 – 38%; $t_{19} = -13.2$, $p < 10^{-9}$). Taken together, oculomotor activity appears to play a role in switching attention between decision alternatives but not when staying focused on the same alternative.

We next assessed the effect of oculomotor activity on the ongoing attention oscillation. We examined how a (micro)saccade occurring between two attentional events affects the respective interval lengths. We found that on average, (micro)saccades decrease the probability for short-latency intervals up to 0.2 s both for staying and switching events (Figure 8G and 8H). Thus, the occurrence of an overt gaze displacement appears to delay the upcoming attentional event. However, the underlying rhythmicity persisted independent from such displacements: We identified post-saccadic rhythmicity (first-to-second peak latency) in 15 out of 20 participants for both event types with no detectable change in oscillation frequency ($t_{14,stay} < 1.8$, $p_{stay} = 0.09$; $t_{14,switch} < 1.1$, $p_{switch} = 0.29$).

In conclusion, oculomotor activity interacted with the way attention switched between decision alternatives. However, overt gaze cannot explain the dynamic aspects of attentional allocation. Thus, the analyses reported in this section indicate that the here presented insights on the dynamics of covert attentional allocation (Figure 3-7) cannot readily be inferred by simply monitoring eye position.

Finally, we assessed how and if attentional saccades are related to neuromodulatory activity. Recent literature highlighted pupil size as a peripheral measure associated with switching attention[37,42]. We thus computed the pupil size as well as the temporal change in size in relationship to the likelihood of attentional saccades (Figure S9). We identified a positive relationship of pupil diameter with the occurrence of stay events (r_{mean} = 0.10, p = 0.004; Figure S9C) as well as a larger pupil diameter during staying (p = 0.005; Figure S9D). Conversely, attention switches were negatively correlated with the change in pupil size (r_{mean} = -0.07, p = 0.01; Figure S9C) and displayed event-triggered pupil constrictions (p = 0.01; Figure S9D). Our findings thus speak against an increase in pupil dilation during attentional switching. Rather, the pupillometric measures here appear to display a more general link to task engagement and information sampling[43-45].

Discussion

Attention likely plays a pivotal role in complex, naturalistic decision-making, steering information sampling in order to assess and compare alternatives. Little has been known about the role of internal attentional dynamics in decision formation. By means of high-precision, continuous tracking of the locus and strength of covert attention in the human brain, we here uncovered rich spontaneous attentional dynamics that governed information sampling during multialternative decisions. We established that the strength of attention fluctuated at a frequency of 11 Hz and that peaks of this attentional oscillation were associated with an increased tendency to maintain focus on a single decision alternative indicative of focal processing. By contrast, troughs of the attentional oscillation were associated with a tendency to switch attention between decision alternatives, indicative of comparative processing. Redirecting attention to another alternative was further preceded by accelerated attentional fluctuations, and reset the ongoing attentional oscillation.

Recent literature has quantified temporal fluctuations in behavioral performance[14,26,28,29,46] and/or in cortical population activity[12-15,26,27,29,36,47], without explicating the information content of the latter. By contrast, we here constructed content-specific decoders from patterns of cortical population activity (trained on independent localizer data). This enabled us to directly track the strength and locus of attention during decision formation. Importantly, this approach enabled us to discover attentional dynamics in an unsupervised fashion, without relying on prior assumptions about rhythmicity or temporal structure. Similar to top-down visual search protocols[23], the framing manipulation in our decision task decoupled the (bottom-up) stimulus intensity from the (top-down) task-relevance of the choice alternatives. We can thus conclude that our findings, and particularly the dominant attention oscillation frequency

at 11 Hz, were not driven by bottom-up sensory cortical responses (compare also Figure S2 & S3).

These findings provide a window into the computational and neural basis of decision-making by alluding to the micromechanisms underlying key decision computations. In decision-theoretic models, central computations such as valuation and comparison are conceptualized in idealized ways and assumed to occur at distinct stages of the decision process[32]. Within our proposed framework, re-focusing attention on a previously attended alternative corresponds to a deep processing mode that could, conceivably, implement valuation. Similarly, switching attention between alternatives may underpin comparative processing. We show that although re-focusing (corresponding to valuation) and switching (corresponding to comparison) of attention peak at different times (Figure S5), effectively they are temporally multiplexed in a single oscillatory cycle. Oscillating attentional strength, a feature potentially established through cortico-thalamic connections[47-50], resolves the competition between focal and comparative processing, or in other words, the conflict between sampling information about each decision alternative and comparing between alternatives[17,28]. Thus, rhythmicity (identified at the level of a single participant) is the mechanism that allows key computations to be performed without competing for the same cognitive resources or substrates[17,18].

One central finding is that stronger attentional rhythmicity is associated with more accurate decisions (Figure 4). We argue that information sampling is improved for brief periods of time as a result of rhythmic attentional gain[51]. At times of strong attentiveness participants were more engaged[43-45] with the task (Figure S9) and more likely to increase processing of the attended decision alternative (Figure 5). Consequently, decision formation processes at the neuronal level might weigh incoming evidence in a similarly time dependent manner[52]. Attention is not static[16,17,28], thus the effect of attention on evidence accumulation is likely dynamic as well. Integrating covert attention as a time-varying variable both in locus as well as strength into existing models[11,39] of evidence

accumulation might thus improve our understanding of dynamic decision making as well as the suboptimalities characterizing behavior in complex, multiattribute contexts[7,11,53].

One prominent aspect of our findings is that, unlike re-focusing, switching events are accompanied by marked changes in neuronal processing. Specifically, the dominant frequency of the attentional oscillation is increased prior to switching (Figure 7). Following a switch event, the phase and the frequency of the attentional oscillation is reset back to 11 HZ, signaling a shift from a disengaged to a focused mode of processing. This reset of the attentional rhythm, speaks for a transient interaction between the two modus operandi of attention, i.e. switching and staying, and is further supported by interactions between the corresponding neural substrates of the two modes (Figure S8 and S9). The reset might serve two purposes. First, it could correspond to an internal go cue[54], indicating readiness of the system to change[20] and briefly enhancing processing power[27,55]. Second, it might temporally align processing at various stages of the functional hierarchy[28,56,57]. In the context of decision theory, an attentional reset and its accompanying neural and attentional dynamics could implement binary comparisons[1,7,39,55,58]. However, further research is needed to better understand the functional role that switching resets have during decision-making.

Finally, our findings suggest that the fast dynamics of sampling information from various decision alternatives are distinct from oculomotor activity. In principle, oculomotor responses, i.e. (micro)saccades, can guide subsequent neuronal processing[21,55,56] by triggering shifts of attention. Indeed, we showed that fixational eye movements and microsaccades had an effect on switching attention between alternatives (Figure 8). Overt gaze displacements yielded a brief post-saccadic suppression of attentional event probability followed by a strengthening of the visual representation of the focused alternative around 0.15 – 0.2 s after a saccade. However, not every covert shift of attention is accompanied by compatible eye-movements[30,31,38]. Particularly, oculomotor activity itself did not display rhythmicity, inter-saccadic intervals

peaked later than attentional event intervals and (micro)saccades displayed a relationship to switching but not to re-focusing attentional events. Lastly, the rhythmicity within the attentional cycle was not affected by overt gaze. Although recent experimental and modeling studies have emphasized the causal role of overt fixations on choice[9,10,39]and intrinsic value representations[11,41], our results paint a more nuanced picture. We show that the relationship between covert information sampling and eye-movements might be a one-way street: microsaccades can elicit covert attentional reorienting, but covert information sampling is not necessarily associated with microsaccades. Thus, where one is fixating and what is intrinsically being processed are not interchangeable units of attention and neuronal processing. Our study offers a methodological framework that dissociates the role that latent and overt attentional components play on decision formation.

In conclusion, our findings highlight rhythmic attention as a general neurophysiological mechanism that resolves conflicts between neuronal processing stages in visual search, target detection, perception and, as shown here for the first time, multialternative decision-making. Focused and comparative sampling of information are multiplexed within an oscillatory cycle of about 0.1 seconds, operating distinctly from overt oculomotor markers. These sampling dynamics challenge extant models of choice, which assume that value information is optimally read-out by downstream areas implementing comparison between alternatives. These insights open new theoretical avenues, highlighting the role of rhythmic information processing in shaping key decision computations.

Acknowledgements

This research was supported by the EU Horizon 2020 Research and Innovation Program (ERC starting grant no. 802905, K.T.) and the BMBF (01GQ1907, T.H.D.)

Author Contributions

All authors contributed to the conceptualization and experimental protocol. M.S., Y.C. & M.T.M. collected the data. M.S. & Y.C. did the formal data analysis and M.S. visualized the results. M.S., T.H.D. & K.T. wrote the initial draft, all authors contributed to editing the manuscript.

Declaration of Interests

The authors declare no competing interests.

Data and Code Availability

Data and Code for reproducing the main results will be deposited on osf.io (under CC 4.0 license) and made publicly available upon publication.

Methods

Participants and experimental procedure

Twenty participants (9 female, age_{mean} = 28.05 years ± age_{STD} 4.6 years) participated in a three-alternative decision-making task with variable task framing. The experiment was approved by the ethics committee of the Hamburg Medical Association and conducted in accordance with the Declaration of Helsinki. All participants gave their written informed consent and received monetary compensation for their participation.

Decision-making task. During central fixation three Gabor patches of varying contrast levels and orientations appeared on screen. The stimuli were presented peripherally (2.2^{o} eccentricity, 1.6^{o} stimulus diameter) at the top and 120° left and right of it. The three stimuli were drawn without replacement from a set of five linearly spaced contrast levels (10 possible combinations). We derived the distance between neighboring contrast levels via a staircase procedure individually within each participant. The patch orientations were drawn from a set of three equally distant orientations with either all three being identical or different. After 1 second into the stimulus presentation a central framing cue (0.3 sec.) indicated the target contrast, either the highest (“Hig”) or lowest (“Low”). We randomized the task framing between trials. After the framing cue offset the central fixation cross re-appeared and initiated a fixed decision phase (2.5 sec.). The three Gabor stimuli were visible and unaltered all throughout the 3.8 seconds stimulus period. After the stimuli turned off the fixation cross rotated 45° and cued the response. Participants had 2 seconds to indicate their decision with a left thumb, right thumb or foot button press for the left, right or top alternative, respectively. We randomized the foot (left or right) between participants. To visually guide the participants we tilted the entire stimulus array 6° clockwise or counter-clockwise when participants were using their right or left foot, respectively. Task framing, contrast levels, Gabor orientation and stimulus locations were fully randomized, yielding a total of 1080 unique trials. The trials were

blocked into random sets of 120 trials and each participants concluded two full randomization runs (18 blocks).

Sensory localizer. Prior to each block of the decision-making task the participants concluded a sensory localizer block. Each block consisted of 90 consecutive 0.35-second presentations of single Gabor stimuli at full contrast with 0.5 seconds inter-trial intervals. Each stimulus was presented with the same size and eccentricity as during the decision-making task. We instructed the participants to ignore the peripheral stimuli and fixate at the center. The participants' task was to detect a flickering of the central fixation cross that could occur randomly at each stimulus, in total 9 times per block, and indicate the detection with a finger button press. We excluded trials with flicker presentation from further analyses. In each block we fully randomized the orientation and the position over the three locations. Each unique stimulus combination was repeated ten times paired once with a central fixation flickering.

Functional data acquisition and preprocessing

Data acquisition. During the experiment the participants were sitting upright in a whole-head magnetoencephalography scanner (MEG; 275 axial gradiometer sensors, CTF Systems Inc.) in a magnetically shielded room. The data was acquired at a sampling rate of 1200 Hz. Each participant's head position was tracked online using three head localization coils (nasion, left/right preauricular points). Additionally, we recorded a 2-channel bipolar electro-oculogram (horizontal and vertical EOG) and a single channel bipolar electro-cardiogram (ECG) to control for cardiovascular and ocular signal artifacts. Eye-movements and pupil diameter were tracked with an MEG-compatible Eyelink 1000 system (SR Research). We further collected T1-weighted structural magnetic resonance images (MRI; sagittal MP-RAGE) to reconstruct individualized high-resolution head models.

Preprocessing. We band-pass filtered the continuous MEG data segments between 0.2 and 200 Hz (4th order Butterworth filter) and down-sampled it to 400 Hz. Next, we filtered

the line noise with a notch filter at 50 Hz and its first 6 harmonics (1 Hz stop-band filter width). We implemented a two-stage procedure for artifact rejection[59,60]: First, we inspected all data segments for technical- (i.e. SQUID-jumps, passing cars), muscle- and eye-blink artifacts and excluded corresponding time intervals from further analyses. Second, we filtered the data into two distinct frequency ranges, a low- from 0.2 to 30 Hz and a high-range from 30 to 200 Hz, with a 4th order Butterworth filter. We computed independent component analyses (ICA) on both frequency ranges separately. This approach takes advantage of the intrinsic properties of different artifact types. On the one hand, eye-blinks eye-movements, passing cars and cardiovascular artifacts display predominantly low-frequency features. On the other hand, muscle activity shows the strongest effects in higher frequencies. We visually inspected the independent components, rejected artifact components based on their topology, power-spectra and time-courses[59]and subsequently recombined both frequency bands.

Spectral analysis and source reconstruction

Spectral analysis. We estimated time-frequency representations of the time-domain MEG signals using Morlet's wavelets[61]. We set the wavelet bandwidth at 0.5 octaves ($f/\sigma_t = 5.83$, kernel width at σ_t) and derived complex spectral estimates for frequencies between 2 to 90.5 Hz in quarter octave steps (2^1 to $2^{6.5}$ Hz).

Source projection. Based on each participants individual structural MRI we generated single-shell boundary-element method models[62](BEM) and computed the physical forward model (leadfields) for 457 equally spaced cortical sources[63,64] (~1.2 cm distance, at 0.7 cm depth below pial surface). Sensor locations, source and leadfield positions were co-registered to the common MNI-space using the position of the three head-localization coils. We applied dynamic imaging of coherent sources[65,66] (DICS) linear beamforming to estimate source-level neuronal activity. DICS is a spatial filtering approach that reconstructs activity at the source of interest with unit gain while at the same time maximally suppressing signal contributions from other sources.

Encoding the focus of covert attention

To reconstruct the focus of covert attention during free information sampling of multiple stimuli we implemented an inverted encoding model[19]. The modeled activity hereby displays momentary changes of the visual representations of the presented stimuli (compare also Figure 2). The model assumes that the sensor-level MEG activity can be described as a weighted sum of distinct abstract neuronal populations, i.e. information channels, with individual tuning properties to the angular positions plus noise *N*[19].

$$MEG_{Loc} = WC_{Loc} + N$$

We trained the encoding model on the functional localizer task MEG_{Loc}. C_{Loc} was a design matrix describing a set of basis functions, i.e. the tuning curves, for each information channel (see Figure 2A) and *W* described the weight matrix specifying the relationship between the information channels and the neuronal data. Each information channel was modelled as a half-wave rectified sinusoidal filter *f* with a fifth power exponent ($\alpha = 5$). We derived the basis functions *f* for the design matrix as

$$f = |cos^{\alpha}[0.5(\theta - \mu)\pi/180]|$$

Here, θ is a continuous variable indicating the angular position relative to central fixation, and μ the preferred angle of each filter (θ and μ are in degrees, with 0° pointing upward along the vertical midline and angular value increasing counter-clockwise e.g., 90° pointing leftward). α was the power exponent set to 5. The target stimuli were set to μ = 0°, 120° and 240° for top, left and right, respectively. During the functional localizer task only one stimulus out of the full set has been visible on screen. Hence, we trained the model during the localizer, as both MEG_{Loc} and C_{Loc} were known variables. We estimated the weight matrix *W* (sensors x information channels) as follows

$$w_k = MEG_{Loc} c_{Loc,k}^T (c_{Loc,k} c_{Loc,k}^T)^{-1}$$

Where w_k denotes the weights of the *kth* information channel $c_{Loc,k}$, i.e. a single tuning curve. As neighboring MEG channels are not independent estimates of neuronal activity

due to volume conduction we further included multivariate noise normalization to improve the pattern reliability[79]. Thus, we transformed each w_k into the pre-whitened weighting vector g_k

$$g_k = \frac{E_k^{-1} w_k}{w_k^T E_k^{-1} w_k}$$

Where E is the noise covariance matrix for channel k using the channels noise term as $\varepsilon_k = MEG_{Loc} - w_k c_{Loc,k}$. E was regularized by shrinking it towards the diagonal matrix, using the optimal shrinkage factor, i.e., minimizing the expected squared loss of the resultant covariance estimator[67]. With the optimized weight-matrix G we can estimate the latent visual representation of the stimuli during the multi-alternative decision-making task (see Figure 2B). Therefore, we invert the encoding model

$$C_{MDM} = G^T MEG_{MDM}$$

C_{MDM} comprises the estimated response as the representational activity distribution over angular positions for each time point during the task. The strength of the representation indexes the covert visual attention towards each target on screen.

Lastly, we reconstructed the momentary spatial focus as the vector sum over the three estimated stimulus activities. The vector orientations were set to 0°, 120° and 240° for the top, left and right stimulus, respectively and the corresponding length at each orientation from the channel response C_{MDM}. This reconstructed attentional vector visualizes two main characteristics of spatial attention, namely the overall attention paid at each time point and from which target information is sampled. We considered the attentional vector length as a proxy of overall attention and the maximum of the angular similarity to the displayed alternatives as the most likely target of covert spatial attention.

We trained the model for different time points during the localizer task with respect to stimulus onset. To achieve the best decoding performance we selected the optimal training epoch using cross-validation (leave-one-block-out, 18 blocks per participant)

within the sensory localizer task. We found decoding strength to peak between 140 to 170 msec post stimulus onset (Figure S1) and averaged the MEG signal over this period to construct the decoding model for the application on the MEG_{MDM} data.

Spectral analysis of attention strength

We computed time-frequency resolved estimates of the attentional vector length to assess the spectral dynamics of attention strength. We band-pass filtered (4th order Butterworth filter) the trialed vector length (f_{sample} = 400 Hz, from -1.5 seconds relative to stimulus onset to 2 seconds after stimulus offset) to center frequencies between 2.8 Hz to 90.5 Hz in quarter octave steps ($2^{1.5}$ to $2^{6.5}$). The pass-band covered the center frequency plus/minus half an octave, e.g. for $2^{1.5}$ Hz center frequency we filtered the data between 2^1 and 2^2 Hz. We estimated the frequency dependent attention strength as the absolute value of the complex Hilbert transform from the time-domain vector length signal. To exclude edge artifacts we cut two cycles of the center frequency from the beginning and end of each trial. We visualized the data between -1.5 to +3 seconds relative to the framing cue onset. We applied the same procedure for the reconstructed stimulus activities at each location (compare Figure S2 and S3).

For the analysis of attention strength fluctuations as a function of correct versus error trials we stratified the included trials. Hereby, we matched the numbers of trials included from each of the 10 possible contrast combinations per framing condition. For all participants we identified more correct choices than error choices in all stimulus combinations. We thus randomly subsampled one hundred times from all correct trials according to the stratification assumptions and averaged the spectral amplitude and the vector length over repetitions before comparing against error trials (see Figure 4).

Defining attentional events

We estimated the momentary focus of spatial attention via the angular similarity of the attentional vector to the three stimuli on screen. At each point in time the attentional vector can display the focus to be close to one or in between targets. The maximum of

the angular similarity (MAS) between the Attentional Vector and the three alternatives is an estimate of how focused a participant is. If MAS equals 1 then the participant is focused solely on one alternative at a given time point. The minimum MAS is 0.5 for the case when the Attentional Vector points exactly in between two alternatives. To investigate the dynamics of information sampling, i.e. when one alternative is selectively focused, we thresholded the maximum angular similarity at the participant-specific 90th percentile over the entire dataset and binarized the time-courses accordingly. However, as the vector orients in circular space and even under completely random conditions will point towards one of the three stimuli at times we added a second threshold on the vector length (90th percentile within a trial). Thus, we recorded attentional events when both thresholds were crossed at the same time. In other words, we traced points in time when participants were both attentive and locked on one stimulus. We recorded the first time point of passing both thresholds as an event onset and excluded events occurring within 0.025 sec after the previous onset.

Event dynamics. To assess the dynamics of these attentional saccades we investigated the intervals between subsequent events. Here, we recorded the time from event *e* onset to the onset of event *e+1* within a trial and generated inter-event-interval (IEI) histograms over all events and trials within a participant. We excluded intervals reaching over trials. The histograms were computed over a median of 17,696 events per participant (range 12,377 to 28,909; compare Figure S4). We further generated Null-models for inference statistical testing using randomization. Hereby, we randomized the trial each event was belonging to while keeping its position within the trial. In other words, when we detected for example 10 events at time point *t* scattered over 2160 trials, we randomly reassigned trial identities to these events (without replacement) and proceeded in the same way with time point *t+1*. We computed the IEI histogram after every randomization run. With this approach we can randomize event relationships

without tempering with the task-dependent dynamics. We repeated the randomization step 1000 times for each participant.

Event sequences. We further tracked first order event sequences. An event can occur either at the same stimulus location as the one before or a different location, i.e. a participant either refocuses (stay) or reorients (switch) their attention. We generated IEI histograms and the randomization for both event types separately and statistically tested interval probabilities against the mean of the randomized Null-models (one-sided paired t-test). Hereby, we obtained t-scores for each interval from 0.025 to 0.5 seconds (at f_{sample} = 400 Hz) for both stay and switch.

Interval-probability fluctuations. If we assume that attention is rhythmic then attentional events would occur probabilistically at preferential phases within an underlying oscillation and we would expect to observe distinct peaks in the IEI histograms: The first peak would display the preferential phase within the first oscillatory cycle, the second peak the second cycle, etc. Thus, we can estimate the prevalent attentional fluctuation frequency as the inverse of the latency between peaks. Therefore, we subtracted the participant-specific expected IEI histogram (Null-model) from the observed histogram. All non-significant values were set to zero according to random-effect statistics based on randomization (one-sided paired t-test against zero, $p < 0.01$; see also above). We smoothed the resulting truncated histograms twice with a 0.01 sec boxcar kernel, padding the edges to the first and last histogram value. Finally, we extracted the local maxima of the truncated and smoothed histograms. Overall, we identified one significant peak in 17 and 18 participants and at least two peaks in 16 and 17 participants for the stay- and switch-IEI histograms, respectively. For further analyses we defined the cycle length of the attention rhythm as the latency from the first to the second peak.

Threshold assessment. We further controlled for effects of the applied threshold through a systematic assessment for a wide range of threshold choices. In theory, if the thresholds are too liberal the analysis will include several random events converging the

IEI histogram to an exponential decay. If the threshold is too high there won't be enough events to have sufficient statistical power for the full IEI distribution. We varied the applied thresholds between the 50% and 95% percentile in 5% steps as well as for the 97.5% and 99% percentile separately for the maximum angular similarity and the vector length (Figure S11). This approach yielded a total of 144 (12 x 12) threshold combinations. We replicated our main findings (individual peaks in the IEI histogram) for a variety of threshold choices between the 80% and 95% percentile (Figure S11A and S11B). Importantly, the timing of histogram peaks appeared to be stable over thresholds. Further, we quantified the deviation of the histogram from an exponential decay, i.e. randomly distributed events, through the variability of interval probabilities further referred to as modulation intensity. Hereby, we first log-transformed the interval probabilities and linearly detrended the resulting values. Next, we smoothed these distributions with a 0.025 second (10 samples) box-car kernel twice and defined local maxima. Finally, we computed the modulation intensity as the standard deviation of the detrended histogram between the first and second maximum (Figure S11C and S11D). We found the strongest median modulation intensity for the highest vector length thresholds at over 95% with variably applicable thresholds for the MAS. Further increasing both thresholds beyond the 95% percentile yielded inconclusive modulation in several participants due to a lack of identifiable events (Figure S11E and S11F). We thus conclude that our main findings are threshold invariant within a sensible range between the 80% to 97.5% percentile with an optimal range approximately between the 90% and 95% percentile for both parameters. At the 90% percentile threshold for both measures, i.e. the applied threshold during the main text, thus granted both reasonably reliable modulation intensity and further a sufficient number of attentional events to increase statistical power for event-triggered analyses (Figure S11G and S11H). Finally, the optimal threshold parameters depend on the research question, the number and the length of the trials. It is thus pivotal to control these parameters for each new analysis.

However, we must stress that optimizing the parameters does not evoke rhythmicity or temporal structure but can only reveal existing structure.

Peri-event fluctuations of attention

To compare the dynamics leading up to attentional events we investigated the event-triggered fluctuations of attention from 0.2 sec before to 0.2 sec after each event. Here, we averaged the attention strength, i.e. attention vector length, and the attention focus, i.e. maximum angular similarity, over all events within each participant and z-scored the traces according to the distribution between -0.2 to -0.03 sec (pre-event period) and 0.03 to 0.2 sec (post-event period) before averaging over participants. We excluded the peri-event period (± 0.03 sec.) from normalization as the event itself, by definition the highest values, would skew the distribution. For further visualization we de-trended and smoothed the event-triggered traces with a 0.025 sec boxcar kernel separately for the pre- and post-event period. Further, we used the de-trended and smoothed traces to define prominent peri-event fluctuation frequencies via the inverse of the average peak-to-peak latencies.

Pupillometry and oculomotor activity analysis

We tracked the eye-gaze and pupil size of the right eye at 1000 Hz sampling rate with an EyeLink 1000 Long Range Mount (SR Research, Osgoode, Canada). We calibrated the eye-tracker at the start of each block. The average spatial resolution was between 15 – 30 min arc. We down-sampled the sampling to 400 Hz compatible to the MEG data. Due to hardware issues we had to exclude one subject from the analysis.

Defining pupil responses. We detected blinks according to the MEG preprocessing pipeline and saccades using the algorithm provided by SR Research with default settings. Within each participant we normalized the average pupil size between the 5% and 95% percentile. We derived the change in pupil diameter as the temporal derivative of the pupil size by subtracting adjacent frames.

Microsaccade detection. We defined microsaccades as brief events of high gaze velocity. We computed gaze velocity as the Euclidean distance in fixation position, i.e. between x- and y-coordinates, over neighboring frames. We further smoothed the velocity with a 0.02 s box-car kernel and z-scored within each trial. Then we defined samples exceeding $z > 3$ as microsaccades. Furthermore, to avoid counting the same event multiple times we imposed a minimum delay of 0.025 s between microsaccades. The microsaccade rate was generated as the saccade probability over trials at each sample multiplied by the sampling rate (400 Hz).

Relating micro- and attentional saccades. We assessed the attentional event-triggered microsaccade rate in time-windows between -0.3 to 0.3 s from attention event onset and averaged over events separately for switch and stay. We compared the average microsaccade rate within these windows against trial-shuffled attention-event definitions (see also above), i.e. the change in microssacade rate. We further analyzed the microsaccade triggered attention strength, i.e. vector length, in a time-window between -0.4 to 0.8 s from microsaccade onset. Finally, we investigated the effect of microsaccades on the rhythmicity of attentional events by re-computing the inter-event-interval histograms separately for intervals containing or not containing a microsaccade.

Neural correlates of covert attentional saccades

We computed the neuronal signal strength, i.e. the amplitude envelope, over the entire cortex to assess the relationship to attentional events (see also Spectral analysis and source reconstruction). According to our results (Figure 3E and 5C) we focused the analysis on the alpha (11 Hz), beta (22 Hz) and gamma (40 Hz) frequency range. According to the literature we further included the theta frequency range (4 Hz)[16,17,28]. Within each participant and source we correlated the frequency-specific signal amplitude envelope with the event probability throughout the stimulus on period. For each event type as well as the difference between them we tested the correlation against zero over

participants (two-sided t-test). We further computed the correlation between the neural signal envelopes and the corresponding band-limited attentional fluctuations.

Event-triggered neural signals. To assess the relationship between event-triggered attention- and neural modulations we averaged over signal amplitudes for switch and stay events separately in each cortical source for a time window of ± 0.3 sec relative to event onset. We z-scored the neuronal activity within each window prior to averaging over events and participants. For visualization purposes we grouped a subset of cortical sources into four regions-of-interest[16,17,28] approximating: early visual areas including V1, medial parietal cortex, medial prefrontal cortex (mPFC) and the dorsolateral prefrontal cortex (dlPFC) including the frontal eye field (FEF)[68]. The average ROI activity was statistically compared between event types using a two-sided paired t-test.

References

1. Gold, J.I., and Shadlen, M.N. (2007). The neural basis of decision making. Annu Rev Neurosci *30*, 535-574. 10.1146/annurev.neuro.29.051605.113038.
2. Donner, T.H., Siegel, M., Fries, P., and Engel, A.K. (2009). Buildup of choice-predictive activity in human motor cortex during perceptual decision making. Curr Biol *19*, 1581-1585. 10.1016/j.cub.2009.07.066.
3. Siegel, M., Buschman, T.J., and Miller, E.K. (2015). Cortical information flow during flexible sensorimotor decisions. Science *348*, 1352-1355.
4. Busemeyer, J.R., Gluth, S., Rieskamp, J., and Turner, B.M. (2019). Cognitive and neural bases of multi-attribute, multi-alternative, value-based decisions. Trends in cognitive sciences *23*, 251-263.
5. Russo, J.E., and Dosher, B.A. (1983). Strategies for multiattribute binary choice. Journal of Experimental Psychology: Learning, Memory, and Cognition *9*, 676.
6. Tsetsos, K., Usher, M., and Chater, N. (2010). Preference reversal in multiattribute choice. Psychological review *117*, 1275.
7. Noguchi, T., and Stewart, N. (2014). In the attraction, compromise, and similarity effects, alternatives are repeatedly compared in pairs on single dimensions. Cognition *132*, 44-56.
8. Noguchi, T., and Stewart, N. (2018). Multialternative decision by sampling: A model of decision making constrained by process data. Psychological review *125*, 512.
9. Krajbich, I., and Rangel, A. (2011). Multialternative drift-diffusion model predicts the relationship between visual fixations and choice in value-based decisions. Proceedings of the National Academy of Sciences *108*, 13852-13857.
10. Orquin, J.L., and Mueller Loose, S. (2013). Attention and choice: a review on eye movements in decision making. Acta Psychol (Amst) *144*, 190-206. 10.1016/j.actpsy.2013.06.003.
11. Krajbich, I. (2019). Accounting for attention in sequential sampling models of decision making. Curr Opin Psychol *29*, 6-11. 10.1016/j.copsyc.2018.10.008.
12. VanRullen, R., Carlson, T., and Cavanagh, P. (2007). The blinking spotlight of attention. Proc Natl Acad Sci U S A *104*, 19204-19209. 10.1073/pnas.0707316104.
13. Busch, N.A., and VanRullen, R. (2010). Spontaneous EEG oscillations reveal periodic sampling of visual attention. Proc Natl Acad Sci U S A *107*, 16048-16053. 10.1073/pnas.1004801107.
14. Landau, A.N., and Fries, P. (2012). Attention samples stimuli rhythmically. Curr Biol *22*, 1000-1004. 10.1016/j.cub.2012.03.054.

15. Fiebelkorn, I.C., Saalmann, Y.B., and Kastner, S. (2013). Rhythmic sampling within and between objects despite sustained attention at a cued location. Curr Biol *23*, 2553-2558. 10.1016/j.cub.2013.10.063.
16. VanRullen, R. (2016). Perceptual Cycles. Trends Cogn Sci *20*, 723-735. 10.1016/j.tics.2016.07.006.
17. Fiebelkorn, I.C., and Kastner, S. (2019). A Rhythmic Theory of Attention. Trends Cogn Sci *23*, 87-101. 10.1016/j.tics.2018.11.009.
18. Fiebelkorn, I.C., and Kastner, S. (2020). Functional Specialization in the Attention Network. Annu Rev Psychol *71*, 221-249. 10.1146/annurev-psych-010418-103429.
19. Brouwer, G.J., and Heeger, D.J. (2009). Decoding and reconstructing color from responses in human visual cortex. Journal of Neuroscience *29*, 13992-14003.
20. Buschman, T.J., and Kastner, S. (2015). From Behavior to Neural Dynamics: An Integrated Theory of Attention. Neuron *88*, 127-144. 10.1016/j.neuron.2015.09.017.
21. Posner, M.I. (2016). Orienting of attention: Then and now. Quarterly journal of experimental psychology *69*, 1864-1875.
22. Mo, C., Lu, J., Wu, B., Jia, J., Luo, H., and Fang, F. (2019). Competing rhythmic neural representations of orientations during concurrent attention to multiple orientation features. Nat Commun *10*, 5264. 10.1038/s41467-019-13282-3.
23. Kienitz, R., Schmid, M.C., and Dugue, L. (2022). Rhythmic sampling revisited: Experimental paradigms and neural mechanisms. Eur J Neurosci *55*, 3010-3024. 10.1111/ejn.15489.
24. Donner, T.H., and Siegel, M. (2011). A framework for local cortical oscillation patterns. Trends Cogn Sci *15*, 191-199. 10.1016/j.tics.2011.03.007.
25. Bellet, J., Chen, C.Y., and Hafed, Z.M. (2017). Sequential hemifield gating of alpha- and beta-behavioral performance oscillations after microsaccades. J Neurophysiol *118*, 2789-2805. 10.1152/jn.00253.2017.
26. Helfrich, R.F., Fiebelkorn, I.C., Szczepanski, S.M., Lin, J.J., Parvizi, J., Knight, R.T., and Kastner, S. (2018). Neural Mechanisms of Sustained Attention Are Rhythmic. Neuron *99*, 854-865 e855. 10.1016/j.neuron.2018.07.032.
27. Peylo, C., Hilla, Y., and Sauseng, P. (2021). Cause or consequence? Alpha oscillations in visuospatial attention. Trends Neurosci *44*, 705-713. 10.1016/j.tins.2021.05.004.
28. Fries, P. (2023). Rhythmic attentional scanning. Neuron *111*, 954-970. 10.1016/j.neuron.2023.02.015.
29. Raposo, I., Szczepanski, S.M., Haaland, K., Endestad, T., Solbakk, A.K., Knight, R.T., and Helfrich, R.F. (2023). Periodic attention deficits after frontoparietal lesions

provide causal evidence for rhythmic attentional sampling. Curr Biol *33*, 4893-4904 e4893. 10.1016/j.cub.2023.09.065.
30. Buschman, T.J., and Miller, E.K. (2009). Serial, covert shifts of attention during visual search are reflected by the frontal eye fields and correlated with population oscillations. Neuron *63*, 386-396. 10.1016/j.neuron.2009.06.020.
31. Gaillard, C., Ben Hadj Hassen, S., Di Bello, F., Bihan-Poudec, Y., VanRullen, R., and Ben Hamed, S. (2020). Prefrontal attentional saccades explore space rhythmically. Nat Commun *11*, 925. 10.1038/s41467-020-14649-7.
32. Platt, M.L., and Plassmann, H. (2014). Multistage Valuation Signals and Common Neural Currencies. In Neuroeconomics, pp. 237-258. 10.1016/b978-0-12-416008-8.00013-9.
33. Hafed, Z.M., and Clark, J.J. (2002). Microsaccades as an overt measure of covert attention shifts. Vision research *42*, 2533-2545.
34. Moore, T., and Armstrong, K.M. (2003). Selective gating of visual signals by microstimulation of frontal cortex. Nature *421*, 370-373.
35. Laubrock, J., Kliegl, R., Rolfs, M., and Engbert, R. (2010). When do microsaccades follow spatial attention? Attention, Perception, & Psychophysics *72*, 683-694.
36. Fiebelkorn, I.C., Pinsk, M.A., and Kastner, S. (2018). A Dynamic Interplay within the Frontoparietal Network Underlies Rhythmic Spatial Attention. Neuron *99*, 842-853 e848. 10.1016/j.neuron.2018.07.038.
37. Wang, C.A., and Munoz, D.P. (2021). Differentiating global luminance, arousal and cognitive signals on pupil size and microsaccades. European Journal of Neuroscience *54*, 7560-7574.
38. Liu, B., Nobre, A.C., and van Ede, F. (2022). Functional but not obligatory link between microsaccades and neural modulation by covert spatial attention. Nat Commun *13*, 3503. 10.1038/s41467-022-31217-3.
39. Krajbich, I., Armel, C., and Rangel, A. (2010). Visual fixations and the computation and comparison of value in simple choice. Nat Neurosci *13*, 1292-1298. 10.1038/nn.2635.
40. Xie, Y., Nie, C., and Yang, T. (2018). Covert shift of attention modulates the value encoding in the orbitofrontal cortex. Elife *7*. 10.7554/eLife.31507.
41. Mormann, M., and Russo, J.E. (2021). Does Attention Increase the Value of Choice Alternatives? Trends Cogn Sci *25*, 305-315. 10.1016/j.tics.2021.01.004.
42. Wang, C.A., and Munoz, D.P. (2015). A circuit for pupil orienting responses: implications for cognitive modulation of pupil size. Curr Opin Neurobiol *33*, 134-140. 10.1016/j.conb.2015.03.018.

43. Dahl, M.J., Mather, M., and Werkle-Bergner, M. (2022). Noradrenergic modulation of rhythmic neural activity shapes selective attention. Trends in cognitive sciences *26*, 38-52.
44. Pfeffer, T., Keitel, C., Kluger, D.S., Keitel, A., Russmann, A., Thut, G., Donner, T.H., and Gross, J. (2022). Coupling of pupil- and neuronal population dynamics reveals diverse influences of arousal on cortical processing. Elife *11*. 10.7554/eLife.71890.
45. Wainstein, G., Whyte, C., Martens, K., Müller, E., Munn, B., Medel, V., Anderson, B., Stöttinger, E., Danckert, J., and Shine, J. (2022). Noradrenergic modulation of whole brain dynamics mediates perceptual switches.
46. Dugue, L., Roberts, M., and Carrasco, M. (2016). Attention Reorients Periodically. Curr Biol *26*, 1595-1601. 10.1016/j.cub.2016.04.046.
47. Fiebelkorn, I.C., Pinsk, M.A., and Kastner, S. (2019). The mediodorsal pulvinar coordinates the macaque fronto-parietal network during rhythmic spatial attention. Nat Commun *10*, 215. 10.1038/s41467-018-08151-4.
48. Saalmann, Y.B., Pinsk, M.A., Wang, L., Li, X., and Kastner, S. (2012). The pulvinar regulates information transmission between cortical areas based on attention demands. science *337*, 753-756.
49. Eradath, M.K., Pinsk, M.A., and Kastner, S. (2021). A causal role for the pulvinar in coordinating task-independent cortico-cortical interactions. J Comp Neurol *529*, 3772-3784. 10.1002/cne.25193.
50. Griffiths, B.J., Zaehle, T., Repplinger, S., Schmitt, F.C., Voges, J., Hanslmayr, S., and Staudigl, T. (2022). Rhythmic interactions between the mediodorsal thalamus and prefrontal cortex precede human visual perception. Nat Commun *13*, 3736. 10.1038/s41467-022-31407-z.
51. Reynolds, J.H., and Heeger, D.J. (2009). The normalization model of attention. Neuron *61*, 168-185. 10.1016/j.neuron.2009.01.002.
52. Wyart, V., de Gardelle, V., Scholl, J., and Summerfield, C. (2012). Rhythmic fluctuations in evidence accumulation during decision making in the human brain. Neuron *76*, 847-858. 10.1016/j.neuron.2012.09.015.
53. Tsetsos, K., Moran, R., Moreland, J., Chater, N., Usher, M., and Summerfield, C. (2016). Economic irrationality is optimal during noisy decision making. Proceedings of the National Academy of Sciences *113*, 3102-3107.
54. van Bree, S., Melcón, M., Kolibius, L.D., Kerrén, C., Wimber, M., and Hanslmayr, S. (2022). The brain time toolbox, a software library to retune electrophysiology data to brain dynamics. Nature Human Behaviour *6*, 1430-1439.
55. Groh, J.M., Schmehl, M.N., Caruso, V.C., and Tokdar, S.T. (2024). Signal switching may enhance processing power of the brain. Trends Cogn Sci. 10.1016/j.tics.2024.04.008.

56. Landau, A.N., Schreyer, H.M., van Pelt, S., and Fries, P. (2015). Distributed Attention Is Implemented through Theta-Rhythmic Gamma Modulation. Curr Biol *25*, 2332-2337. 10.1016/j.cub.2015.07.048.
57. Stine, G.M., Trautmann, E.M., Jeurissen, D., and Shadlen, M.N. (2023). A neural mechanism for terminating decisions. Neuron *111*, 2601-2613. e2605.
58. Hunt, L.T., Malalasekera, W.M.N., de Berker, A.O., Miranda, B., Farmer, S.F., Behrens, T.E.J., and Kennerley, S.W. (2018). Triple dissociation of attention and decision computations across prefrontal cortex. Nat Neurosci *21*, 1471-1481. 10.1038/s41593-018-0239-5.
59. Hipp, J.F., and Siegel, M. (2013). Dissociating neuronal gamma-band activity from cranial and ocular muscle activity in EEG. Front Hum Neurosci *7*, 338. 10.3389/fnhum.2013.00338.
60. Siems, M., Pape, A.A., Hipp, J.F., and Siegel, M. (2016). Measuring the cortical correlation structure of spontaneous oscillatory activity with EEG and MEG. Neuroimage *129*, 345-355. 10.1016/j.neuroimage.2016.01.055.
61. Goupillaud, P., Grossmann, A., and Morlet, J. (1984). Cycle-octave and related transforms in seismic signal analysis. Geoexploration *23*, 85-102.
62. Oostenveld, R., Fries, P., Maris, E., and Schoffelen, J.-M. (2011). FieldTrip: open source software for advanced analysis of MEG, EEG, and invasive electrophysiological data. Computational intelligence and neuroscience *2011*, 156869.
63. Hipp, J.F., Hawellek, D.J., Corbetta, M., Siegel, M., and Engel, A.K. (2012). Large-scale cortical correlation structure of spontaneous oscillatory activity. Nat Neurosci *15*, 884-890. 10.1038/nn.3101.
64. Siems, M., and Siegel, M. (2020). Dissociated neuronal phase-and amplitude-coupling patterns in the human brain. NeuroImage *209*, 116538.
65. Van Veen, B.D., Van Drongelen, W., Yuchtman, M., and Suzuki, A. (1997). Localization of brain electrical activity via linearly constrained minimum variance spatial filtering. IEEE Transactions on biomedical engineering *44*, 867-880.
66. Gross, J., Kujala, J., Hämäläinen, M., Timmermann, L., Schnitzler, A., and Salmelin, R. (2001). Dynamic imaging of coherent sources: studying neural interactions in the human brain. Proceedings of the National Academy of Sciences *98*, 694-699.
67. Ledoit, O., and Wolf, M. (2004). A well-conditioned estimator for large-dimensional covariance matrices. Journal of multivariate analysis *88*, 365-411.
68. Hipp, J.F., and Siegel, M. (2015). BOLD fMRI correlation reflects frequency-specific neuronal correlation. Current Biology *25*, 1368-1374.